Atmos. Meas. Tech., 4, 659–667, 2011
www.atmos-meas-tech.net/4/659/2011/
doi:10.5194/amt-4-659-2011

Atmospheric Measurement Techniques

Retrieval of ozone profiles from GOMOS limb scattered measurements

S. Tukiainen[1], E. Kyrölä[1], P. T. Verronen[1], D. Fussen[2], L. Blanot[3], G. Barrot[3], A. Hauchecorne[4], and N. Lloyd[5]

[1]Finnish Meteorological Institute, Helsinki, Finland
[2]Belgian Institute for Space Aeronomy, Brussels, Belgium
[3]ACRI-ST, Sophia-Antipolis, France
[4]Laboratoire Atmosphéres, Milieux, Observations Spatiales (LATMOS), Verriéres-le-Buisson, France
[5]University of Saskatchewan, Saskatoon, Canada

Received: 26 August 2010 – Published in Atmos. Meas. Tech. Discuss.: 8 October 2010
Revised: 18 March 2011 – Accepted: 23 March 2011 – Published: 4 April 2011

Abstract. The GOMOS (Global Ozone Monitoring by Occultation of Stars) instrument on board the Envisat satellite measures the vertical composition of the atmosphere using the stellar occultation technique. While the night-time occultations of GOMOS have been proven to be of good quality, the daytime occultations are more challenging due to weaker signal-to-noise ratio. During daytime GOMOS measures limb scattered solar radiation in addition to stellar radiation. In this paper we introduce a retrieval method that determines ozone profiles between 20–60 km from GOMOS limb scattered solar radiances. GOMOS observations contain a considerable amount of stray light at high altitudes. We introduce a method for removing stray light and demonstrate its feasibility by comparing the corrected radiances against those measured by the OSIRIS (Optical Spectrograph & Infra Red Imaging System) instrument. For the retrieval of ozone profiles, a standard onion peeling method is used. The first comparisons with other data sets suggest that the retrieved ozone profiles in 22–50 km are within 10% compared with the GOMOS night-time occultations and within 15% compared with OSIRIS. GOMOS has measured about 350 000 daytime profiles since 2002. The retrieval method presented here makes this large amount of data available for scientific use.

Correspondence to: S. Tukiainen
(simo.tukiainen@fmi.fi)

1 Introduction

During the last few decades, extensive research efforts have been made to measure the vertical composition of the Earth's atmosphere. Numerous satellite instruments have been deployed specifically to observe the middle atmosphere using different measurement techniques, geometries, and wavelengths regions. Limb-viewing instruments can directly observe the solar or stellar signal as the source is occulted by the atmosphere or instead measure the scattered indirect sunlight (radiance) and various atmospheric emissions.

Compared to the nadir looking instruments the limb-viewing technique can not achieve as good horizontal spatial resolution but it yields superior vertical resolution. The limb view also offers greater sensitivity to trace constituents than the nadir view. Cloud interference is often a disadvantage in the limb view, but on the other hand it can be used, for example, to study polar mesospheric clouds and noctilucent clouds (Petelina et al., 2006; Robert et al., 2009; Pérot et al., 2010). A detailed information of the past and present middle atmosphere instruments can be found e.g. in Grant (1989); Shepherd (2002); Qu et al. (2006).

The obvious advantage of satellite measurements is that large quantities of global data can be gathered over long periods of time. Recent middle atmosphere studies, for instance, Jones et al. (2009); Kyrölä et al. (2010); Kiesewetter et al. (2010); Gillett et al. (2011), have increasingly aimed to utilize and sometimes to combine large satellite data sets in order to understand how ozone (or other species) are changing in time. The goal is to distinguish between natural variations

Published by Copernicus Publications on behalf of the European Geosciences Union.

and anthropogenic forcings in the atmosphere. Furthermore, long and consistent satellite data sets are crucial for validation of climate models.

The GOMOS (Global Ozone Monitoring by Occultation of Stars) instrument on board the Envisat satellite uses the stellar occultation method to probe the atmosphere between 10 and 130 km. Since 2002, GOMOS has performed altogether almost one million measurements. The ozone profiles obtained from the night-time occultations are considered to have typically better than 5% accuracy in the stratosphere (Meijer et al., 2004; Renard et al., 2008; van Gijsel et al., 2010). However, the majority of the daytime ozone profiles retrieved from occultations are currently of poor quality and not suitable for scientific use.

In addition to the star signal, GOMOS also records the limb scattered sunlight during the daytime in similar way to e.g. OSIRIS (Optical Spectrograph & Infra Red Imaging System) on the Odin satellite (Llewellyn et al., 2004) and SCIAMACHY (SCanning Imaging Absorption SpectroMeter for Atmospheric CHartographY) on Envisat (Gottwald et al., 2006). The first experiment to retrieve ozone profiles from the GOMOS bright limb (GBL) measurements was done by Taha et al. (2008), obtaining promising results. In this paper we present a study to retrieve ozone from the GOMOS radiances and show some initial comparison results.

2 GOMOS radiance measurements

2.1 The GOMOS instrument

GOMOS is a UV-visible spectrometer covering the wavelength range from 250 to 675 nm with 1.2 nm spectral resolution (during night-time observations). Two additional infrared channels at 756–773 nm and at 926–952 nm with 0.2 nm spectral resolution are also included. GOMOS is also equipped with two fast photometers sampling at the frequency of 1 kHz in the ranges 644–705 nm and 466–528 nm. GOMOS was designed to measure about 180 different stars as they occultate through the atmosphere. About 300–400 occultation events are recorded each day between around 10–130 km.

The vertical sampling distance of GOMOS is 0.5–1.6 km. The uncertainty in the tangent height registration is very small because stars are point sources whose positions are well known. The only uncertainties come from the satellite position and the ray path calculation but the impact of these on the retrieved profiles is considered negligible (Tamminen et al., 2010).

During the daytime, the GOMOS CCDs record light from the limb using three spatial bands. The central band measures the sum of the star and the limb scattered signal, while the upper and the lower bands measure only the limb contribution. In the operational occultation retrieval, the upper/lower band radiance is removed from the central band measurement to get the pure star signal which is then used for the retrievals. This procedure is performed for the day and twilight observations but not for the night measurements when no limb scattered light contribution is present.

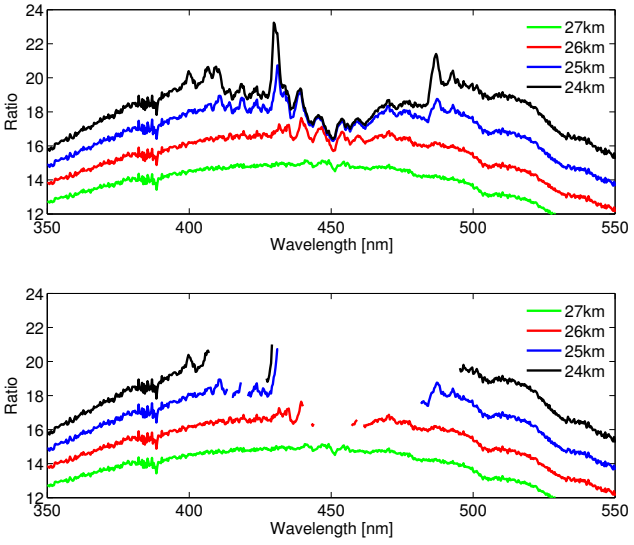

Fig. 1. Saturation in the normalized GOMOS radiances for a few altitudes. Upper panel: current Level 1 version, where obviously saturated pixels are not flagged. Lower panel: forthcoming Level 1 version including improved saturation flags (data achieved via private communications with Gilbert Barrot, ACRI-ST).

2.2 Saturation

The GOMOS radiance measurements suffer from CCD saturation below 30 km in the 400–500 nm band. The saturated pixels are flagged in the Level 1 data but the flags are not correctly implemented in the version 5.00 of the Level 1 data. The effect of the saturation is clearly seen when looking at normalized radiances (measured radiances divided by a radiance spectrum from a high altitude). A normalized radiance is also called *radiance ratio*. Figure 1 shows normalized radiances between 350 and 550 nm for a single scan (orbit 9758, star 83) and for a few altitudes. The upper panel is plotted using the current Level 1 data, and while the signal notably begins to saturate at 26 km, the version 5.00 flags are wrongly claiming the data to be good down to 24 km.

The new Level 1 processing version, coming out in 2011, includes improved saturation flags. The lower panel of Fig. 1 reveals that almost all saturated pixels are now flagged correctly. It is important to have correct saturation flags for a successful retrieval. Our strategy in the retrieval is to take advantage of the whole UV-Visible optical region between 280–700 nm and use dozens or even hundreds of wavelengths. This way the profiles can be retrieved for a wide altitude range. If the saturation flags are incorrect, and also saturated pixels are used in the retrieval, errors in the retrieved

profiles will greatly increase. In this study, we ignored the whole 400–500 nm region to make sure that no saturated pixels were used in the retrieval.

2.3 Stray light

In addition to the CCD saturation, the GOMOS limb scatter measurements suffer from severe stray light contamination. External stray light refers to the light whose origin is outside of the nominal field of view of the slit but is nevertheless observed by the instrument. There are two major sources of the external stray light in GOMOS. One is the solar light scattered by some Envisat hardware into the baffle and optics of GOMOS. The other is the off-axis scattering coming from the sun-illuminated atmosphere. The latter stray light component is most probably coming from the zone below the line of sight between the tangent point and the satellite position. Our preliminary investigations show that there seems to be a positive correlation between cloudiness in this area and the amount of stray light, specially at the red end of the spectrum.

In Taha et al. (2008), the GOMOS stray light was modeled by assuming the measured radiances to be entirely stray light between 80 and 120 km and by doing a simple linear fit for each wavelength. A similar approach was also used by Rault (2005) for SAGE III limb scatter. In this study, the stray light removal method is slightly different. We only consider altitudes above 100 km and use the spectral shape of stray light to constrain a polynomial fit.

The relative amount of stray light in the GOMOS radiances increases with the altitude and above 100 km we consider the signal to be pure stray light. We can deduce the altitude dependence of the GOMOS stray light from the >100 km spectra, but the extrapolation to lower tangent heights will often lead to unreliable results. To avoid this, we constrain the extrapolation by the spectral shape of the stray light. Our stray light correction method consists of the following steps:

1. Calculate the mean relative stray light spectrum

$$S(\lambda) = \frac{1}{n}\sum_{j=1}^{n}\frac{I(\lambda, j)}{I(\lambda_{500}, j)}, \quad (1)$$

where $I(\lambda, j)$ are the measured radiance spectra and $I(\lambda_{500}, j)$ are the measured radiances at 500 nm. The tangent height index j goes through the measurements above 100 km and λ denotes wavelength. Typically, GOMOS begins to scan at ∼130 km with ∼1 km vertical sampling so that the number of $I(\lambda, j)$ spectra is about 30.

2. Compute a linear least squares fit for each wavelength using the measurements above 100 km as the fitting range.

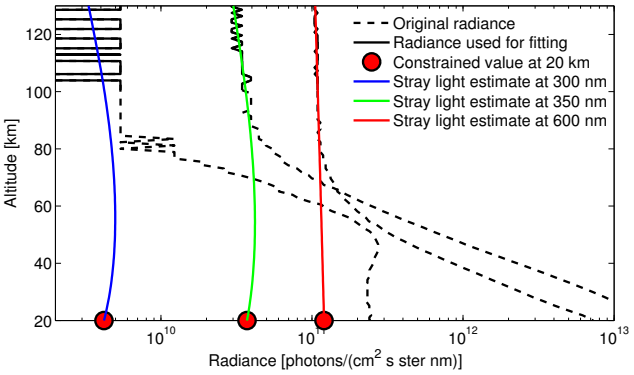

Fig. 2. Stray light estimation for 300 nm, 350 nm, and 600 nm. The spectral shape of the stray light is used to calculate the 20 km points (red circles), which are then used together with the >100 km radiance values to calculate the stray light estimates for all altitudes.

3. Extrapolate this stray light estimate for the 20 km tangent height corresponding to the typical lowest tangent height of the daytime GOMOS scans. We denote these extrapolated 20 km values as $\hat{I}_{\text{ext}}(\lambda)$.

4. Recalculate the extrapolated stray light estimates at 20 km, obtained in the previous step, using the spectral shape $S(\lambda)$ as a constraint. The best fit in the least squares sense is

$$c = \frac{S(\lambda)^T}{S(\lambda)^T S(\lambda)}\,\hat{I}_{\text{ext}}(\lambda). \quad (2)$$

The constrained values at 20 km are then

$$\hat{I}_{\text{fit}}(\lambda) = c\,S(\lambda). \quad (3)$$

5. Compute a third degree least squares polynomial fit for each wavelength using the measurements above 100 km and the recalculated 20 km values $\hat{I}_{\text{fit}}(\lambda)$.

6. Evaluate the polynomial for all measurement tangent heights and subtract the obtained stray light estimate from the radiances.

Figure 2 illustrates the stray light calculation for three wavelengths. The red circles are the constrained 20 km values calculated in Eq. (3). Blue, green, and red lines show the final stray light estimates which are subtracted from the radiances.

A few things should be noted about this algorithm. Because the >100 km spectra always contain some noise and wavelengths are treated independently radiances become noisier after the correction. Another issue is that the optimal range and orders for the the polynomial fits are unknown and the choices can affect the results, too. In this study, we used a linear fit in Step 2 and a third degree polynomial in Step 5. Also, in reality, the amount of stray light may actually vary as

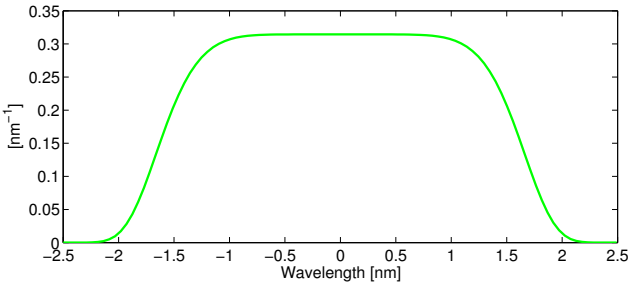

Fig. 3. GOMOS slit function.

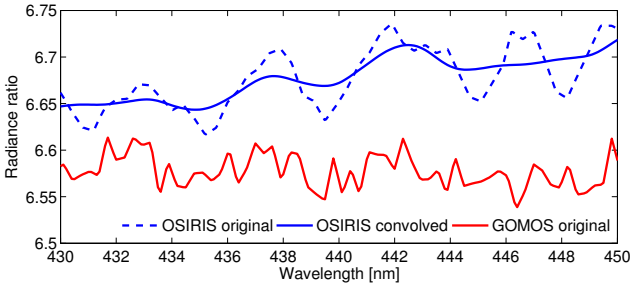

Fig. 4. Comparison of GOMOS and OSIRIS spectral resolution in the NO_2 retrieval region. Shown are 32 km radiances normalized with the 47 km spectra. The GOMOS ratio is before stray light correction and scaled to fit in the figure.

a function of altitude leading to abnormal results from the extrapolations. As mentioned earlier, the GOMOS stray light is dependent on the albedo of the underlying reflective surface between the tangent point and the satellite position. Thus, strong albedo gradients during the measurement can disturb the usually quite linear altitude dependence of stray light at high tangent heights. In these cases, a simple linear fit would probably be better than any higher degree polynomial.

3 Radiance comparison

In this section we compare GOMOS radiances with OSIRIS radiances. OSIRIS is a combined UV-Visible optical and infrared instrument dedicated to limb scatter measurements. The instrument is flying on board the Odin satellite, launched in 2001. The OSIRIS Level 1 data is the latest version, reprocessed in the end of 2009. OSIRIS radiances are relatively free of stray light below ∼70 km and therefore OSIRIS is a good reference for the validation of GOMOS radiances and the stray light correction algorithm. However, it should be noted that stray light is not totally absent from the OSIRIS measurements either. But according to Llewellyn et al. (2004) and references in it, the contamination is rather small and within expected limits. The GOMOS Level 1 is also the most recent available version 5.00 from 2006.

The criteria shown in Table 1 were used to find coincident measurements between GOMOS and OSIRIS. Using the data from the year 2004, a total of 14 matching observations were found when applying the coincidence criteria and excluding data with solar zenith angle larger than 86°. These observations are from a very narrow latitude band around 60° S from January and February 2004.

Table 1. Coincidence criteria for the GOMOS and OSIRIS radiance matches.

Latitude	3°
Longitude	6°
Time	24 h
Sun zenith angle	2°
Scattering angle	2°

3.1 Spectral resolution and noise

The spectral resolution of the GOMOS radiance measurements is ∼3.5 nm, i.e. relatively low compared to ∼1 nm of OSIRIS. The wider slit of GOMOS allows the tracking of occultating stars but it lowers the spectral resolution. Therefore, we convolved the OSIRIS spectra with the GOMOS slit function. The best estimate of the slit function is shown in Fig. 3. The GOMOS slit function was estimated from the GOMOS data by investigating the oxygen emission line at 557 nm whose spectral characteristics are well known.

In addition to the low spectral resolution, the GOMOS radiances are also much noisier than those of OSIRIS. This makes it challenging to retrieve trace gases whose absorption fingerprints are relatively small compared to the ozone fingerprint. For example, NO_2 is routinely retrieved from the OSIRIS data using the NO_2 absorption features in the 430–450 nm region. Figure 4 shows radiance ratios in this region for GOMOS and OSIRIS at 32 km. The absorption lines are barely recognizable in the GOMOS ratio, while the OSIRIS ratio is far cleaner. At higher altitudes the noise in GOMOS obscures the absorption lines even further and below ∼30 km the region begins to saturate as shown in Fig. 1.

3.2 Absolute radiance

First, we analyzed the differences between GOMOS and OSIRIS absolute radiances. The radiances were interpolated in wavelength and in altitude using linear interpolation. Radiance as a function of altitude changes non-linearly in the UV wavelengths but the high vertical sampling of both instruments (1–2 km) allows us to use linear interpolation.

Figure 5 shows an example of an individual OSIRIS (orbit 15702, scan 25) and GOMOS (orbit 9778, star 83) match. At 55 km the amount of stray light in the GOMOS radiance is prominent, especially in the wavelengths above 400 nm. After the stray light removal, the overall agreement

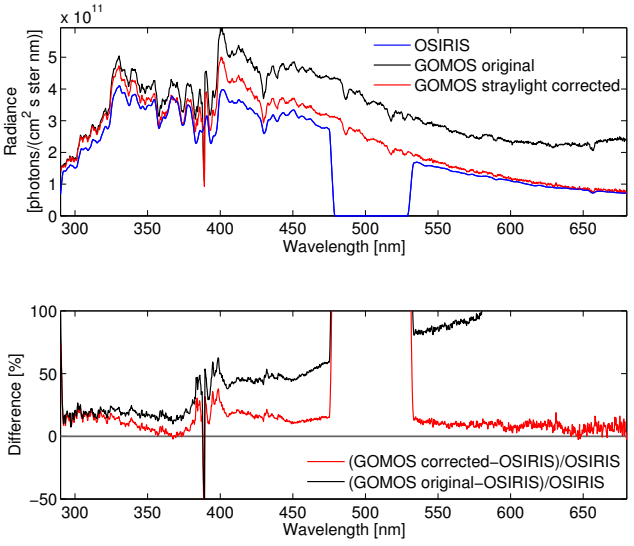

Fig. 5. Example of absolute radiances from GOMOS and OSIRIS. Upper panel: radiances at 55 km. Lower panel: relative differences.

is significantly better but the removal algorithm has introduced some additional noise to the radiance.

Figure 6 presents median differences between OSIRIS and stray light corrected GOMOS radiances for two different altitudes (55 and 30 km). There seems to be a positive bias in the GOMOS radiance below 350 nm. The bias is increasing towards lower altitudes, being up to around 20% at 55 km and 40–60% at 30 km.

3.3 Radiance ratio

Instead of using absolute radiances, a common practice to counteract uncertainties from calibration and polarization is to normalize radiance spectra by a high altitude measurement. It may be a full spectrum from one altitude, typically around 50 km, or the reference can come from various altitudes depending on the wavelength.

The same match as in Fig. 5 is shown in Fig. 7 but the radiances are now normalized with the 47 km spectra. The difference in the UV band is apparent and the stray light corrected ratio is noisier than the original GOMOS radiance ratio. Otherwise the agreement between the OSIRIS ratio and the stray light corrected GOMOS ratio is good.

The median of the differences of the 14 matches is shown in Fig. 8 for 55 and 30 km. At 30 km the GOMOS ratio is biased up to +20% below 320 nm and there is an opposed bias at 55 km. At 55 km the red end of the spectrum is quite noisy due to the stray light correction. The bias in the wavelengths 320–680 nm is 5–10% for both investigated altitudes.

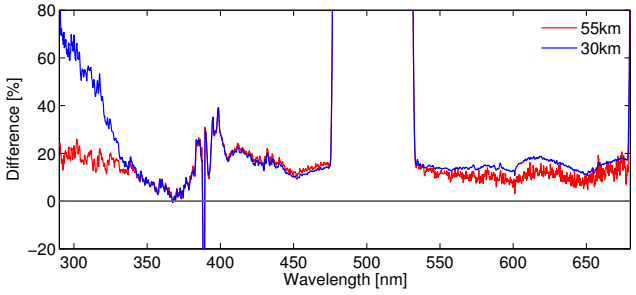

Fig. 6. Median relative difference of the 14 OSIRIS and stray light corrected GOMOS absolute radiances at 30 km (blue) and 55 km (red).

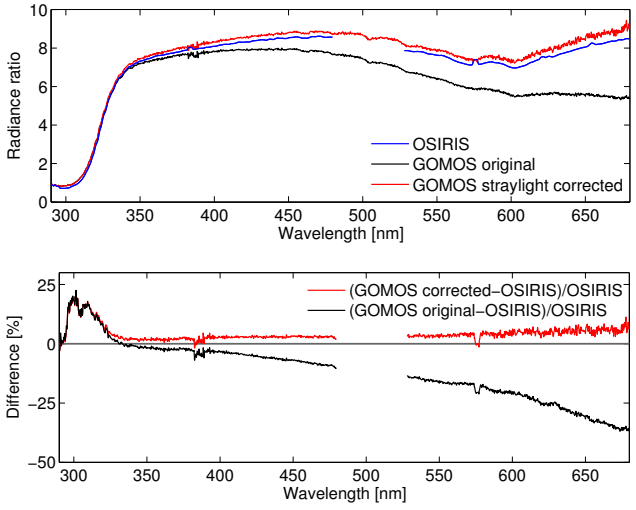

Fig. 7. Example of radiance ratios from GOMOS and OSIRIS. Upper panel: ratios of 30 and 47 km. Lower panel: relative differences.

4 Inversion method

A slightly revised version of the inversion method described in detail in Tukiainen et al. (2008) is used for the retrieval. The fundamental idea is the same. For every measurement tangent height j, a least squares fit weighted by the standard deviation of the noise term is done between the model and the measurement:

$$\frac{I(j,\lambda)}{I_{\mathrm{ref}}(\lambda)} = \frac{\hat{I}_{\mathrm{ss}}(j,\lambda,\rho)}{\hat{I}_{\mathrm{ref}}(\lambda)} R(j,\lambda) + \epsilon, \tag{4}$$

where $I(j,\lambda)$ is the observed radiance and $I_{\mathrm{ref}}(\lambda)$ is the reference measurement at ∼47 km. On the right hand side, $\hat{I}_{\mathrm{ss}}(j,\lambda,\rho)$ is the modeled single scattering radiance, adjusted dynamically during the fitting operations and $\hat{I}_{\mathrm{ref}}(\lambda)$ is the modeled reference radiance including multiple scattering. The second term on the right:

$$R(j,\lambda) = \frac{\hat{I}_{\mathrm{tot}}(j,\lambda)}{\hat{I}_{\mathrm{ss}}(j,\lambda)} \tag{5}$$

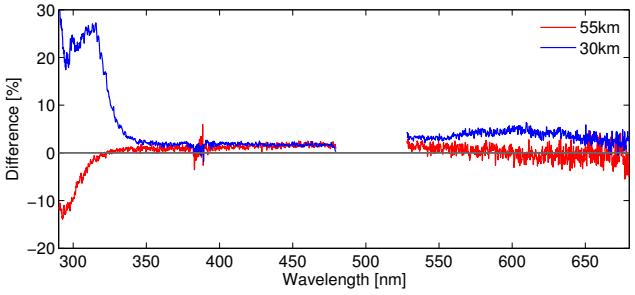

Fig. 8. Median relative difference of the 14 OSIRIS and stray light corrected GOMOS radiance ratios at 30 km (blue) and 55 km (red). Radiances were normalized with the 47 km spectrum.

is the ratio of modeled total to single scattering radiance. This term comes from a look-up-table (see Table 2 and Sect. 4.1) and is kept fixed during iterations. The iterative fitting of the gas densities ρ in Eq. (4) is done using the Levenberg-Marquardt method (Levenberg, 1944; Marquardt, 1963). The standard deviation of ϵ in Eq. (4) is used as a weight in the fitting. At every tangent height, the best fit is the one that minimizes the chi square value

$$\chi^2 = (T_{\text{obs}} - T_{\text{mod}})^T \, \mathbf{C}^{-1} \, (T_{\text{obs}} - T_{\text{mod}}), \quad (6)$$

where T_{obs} is the measurement ratio (left hand side of Eq. 4) and T_{mod} is the modeled ratio (right hand side of Eq. 4 without the error term). The covariance matrix **C** is diagonal and includes only the standard deviation of the measurement error. The standard deviation of the radiance $I(j, \lambda)$ is approximated as

$$\sigma_{\text{rad}}(j, \lambda) = \sqrt{I_e(j, \lambda) + I_{\text{sc}}(\lambda) + I_{\text{dc}}(\lambda)} \, Z(\lambda), \quad (7)$$

where $I_e(j,\lambda)$ is the uncorrected radiance as electrons, $I_{\text{sc}}(\lambda)$ is the approximate variance of the stray light estimate, $I_{\text{dc}}(\lambda)$ is the contribution from the dark charge, and $Z(\lambda)$ is the radiometric sensitivity curve to convert the values into physical units. The variance of the radiance ratio $\frac{I(j,\lambda)}{I_{\text{ref}}(\lambda)}$ is approximated as

$$\sigma^2_{\text{ratio}}(j,\lambda) = \left(\frac{\sigma_{\text{rad}}(j,\lambda)}{I_{\text{ref}}(\lambda)}\right)^2 + \left(\frac{R(j,\lambda)\sigma_{\text{rad}}(j_{\text{ref}},\lambda)}{I_{\text{ref}}(\lambda)}\right)^2, \quad (8)$$

where $I_{\text{ref}}(\lambda)$ is the measurement reference radiance, $R(j, \lambda)$ is the modeled tot/ss ratio, and $\sigma_{\text{rad}}(j_{\text{ref}}, \lambda)$ is the standard deviation of the radiance at the reference altitude. At the moment, no modeling error is added in the covariance matrix **C**.

The atmosphere between around 60 and 20 km is "peeled" from top to down to get the vertical profiles of retrieved species. With this approach, it is possible to retrieve several species simultaneously. Typically O_3, aerosols and neutral air are inverted together using tens (or hundreds) of wavelengths in the 280–680 nm band, while NO_2 is taken from a climatology and kept fixed. In this study we used 71 wavelengths. As shown in Tukiainen et al. (2008), it is better to retrieve minor absorbers such as NO_2 in separate peeling loops using much more narrow wavelength windows. It should be noted that, as mentioned earlier, NO_2 is not currently retrieved from the GOMOS bright limb measurements due to weak spectral performance in the 430–450 nm band of GOMOS. In this study, we did retrieve neutral air and aerosols in the same peeling loop as ozone but the quality of these two products will be determined in later studies.

Table 2. Siro look-up table parameters.

Parameter	Range
Zenith angle	40–90°, 5° resolution
Azimuth angle	20–180°, 10° resolution
Albedo	3 albedos: 0.1, 0.5, 0.9
Climatology	5 regions: tropic, mid latitudes (summer,winter), arctic (summer), Antarctica (summer)
Altitude	12, 14, 16, 18, 21, 23, 25, 27, 30, 35, 40, 50, 60, 70 km
Wavelength	123 wavelengths in the 280–680 nm band

4.1 Radiative transfer model

It is straightforward and computationally very effective to calculate single scattering radiances in limb-viewing geometry. But in the visible wavelengths, a significant part of the photons have scattered multiple times before observed by the instrument. This makes the modeling challenging, and usually approximations are used to simplify the radiative transfer calculations.

Several models have been developed to calculate the multiple scattering radiance in the UV visible wavelengths. Recent models include e.g. SASKTRAN (Bourassa et al., 2008), McSCIA (Spada et al., 2006), Sciatran (Rozanov et al., 2005), MCC++ (Postylyakov, 2004), LIMBTRAN (Griffioen and Oikarinen, 2000) and Siro (Oikarinen et al., 1999).

We use a revised version of the Monte Carlo (MC) model Siro. Siro is a backward MC model – photons are simulated from the detector towards the atmosphere. The latest Siro version is written in Fortran90 and parallelized using OpenMP framework. Options for polarization and refraction are available, but were not used in this study.

The execution time of Siro depends mainly on the tangent point altitude and wavelength. More multiple scattering means slower execution. The multiple scattering contribution is determined by the solar angles, atmospheric composition and albedo.

The running time and the precision of the solution are naturally proportional to the number of simulated photons. With a modern CPU (Xeon E5420) using only a single core, a

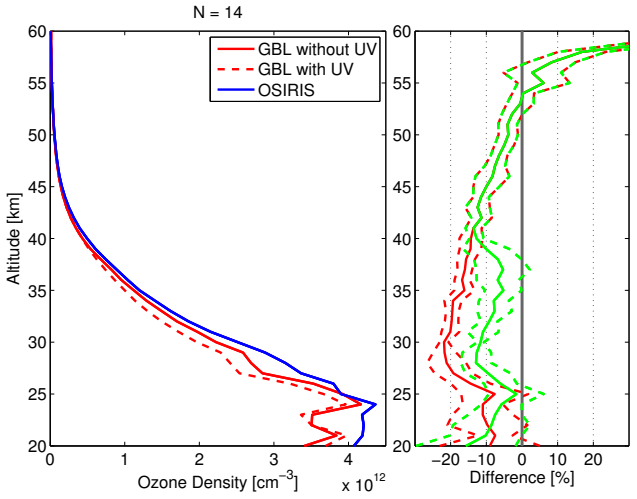

Fig. 9. Retrieved ozone profiles from the 14 GOMOS and OSIRIS radiances of Figs. 6 and 8. Left panel: medians of the OSIRIS profiles (blue), GOMOS profiles retrieved with the UV band (red dashed profile) and without using the UV band below 40 km (red solid profile). Right panel: medians of individual relative differences compared to the OSIRIS profiles and the 25th and 75th percentiles. The red lines show the difference (and deviation) when using the UV band and the green lines show the difference when the UV band is not used.

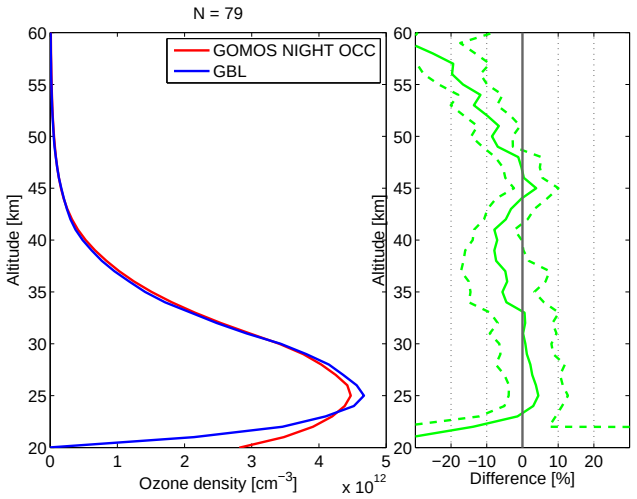

Fig. 10. Comparison of the 79 GOMOS bright limb profiles and GOMOS night occultations at the equator. Left panel: medians of the distributions. Right panel: median of the individual relative differences (solid) and the 25th and 75th percentiles (dashed).

10^5 photon simulation for one wavelength takes a few seconds in the UV region. In the visible band, a similar simulation takes typically around 30 s.

It is computationally too expensive to use Siro directly in the operational retrieval. Instead in Eq. (4), we use a fast analytical single scattering model and perform multiple scattering correction using a Siro calculated look-up table. The Siro look-up table is built with the parameters shown in Table 2. The sensitivity of the look-up table values to the parameters were also studied, and the ranges shown in Table 2 were found sufficient. To get approximately 1% accuracy, radiances were simulated with 10^5 photons.

5 Ozone profile comparison

As there is some discrepancy in the GOMOS and OSIRIS radiances below ∼350 nm, differences in retrieved ozone profiles should be expected. Above around 40 km, these wavelengths are required for successful ozone retrievals. But at lower altitudes, information mainly comes from the Chappuis band around 600 nm, and the UV band can be suppressed from the inversion.

Figure 9 shows a comparison of the 14 GOMOS bright limb and OSIRIS ozone profiles retrieved using the radiances shown in Figs. 6 and 8. The profiles were first interpolated into the same 1 km grid and the medians of the distributions are shown in the left panel. The GOMOS profiles were retrieved with the UV band (red dashed line) and without the UV band below 40 km (red solid line). The right panel shows the medians of the individual relative differences (with OSIRIS being the reference) and the 25th and 75th percentiles. In both cases there is a negative bias below 50 km compared to OSIRIS but flagging the UV wavelengths clearly improves the agreement.

To better test the statistical accuracy of the retrieved profiles, we compare the GOMOS bright limb profiles with the GOMOS night-time occultation profiles. Due to issues in the 400–500 nm band (saturation) and in the UV band below 40 km, we flagged these wavelengths from the retrieval. Figure 10 shows the result of the comparison in the equator between 30° S and 30° N. The 79 profiles are from 2003 with no more than 1° difference in latitude, 2° in longitude and 15 h in time. The median of the individual relative differences is less than 10% between 22 and 50 km. Above 45 km the diurnal variation of ozone starts to take effect, and the GBL values (day) are smaller than the night occultation values, as expected. There is a large bias in the GBL profiles below 22 km compared with the night occultation profiles. This is probably because some saturated pixels were still used in the retrieval (outside of the 400–500 nm band). However, GOMOS daytime profiles at the equator seldom reach to 20 km or lower. During the daytime, when the limb scattering contribution is present, it is difficult to follow occultating stars at low tangent heights. The limb signal starts to overwhelm the star signal and the star tracker loses control more easily.

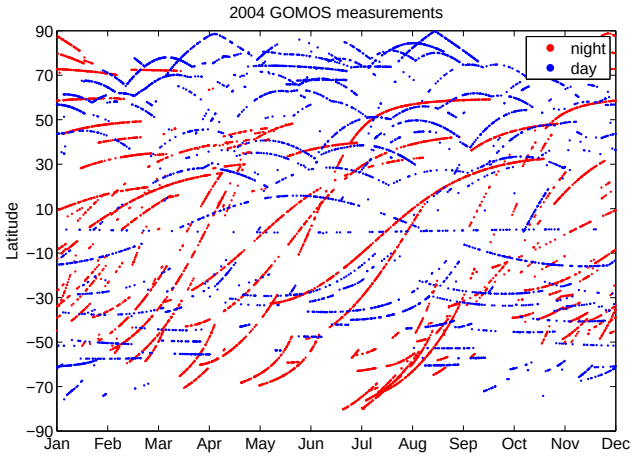

Fig. 11. Distribution of the night and daytime measurements from GOMOS during 2004.

6 Discussion

There are serious defects in the GOMOS Level 1 bright limb data that complicate trace gas retrievals. The stray light contamination is a severe problem at high altitudes. In the wavelengths >400 nm, stray light accounts for as much as 10–50% of the measured signal already at 55 km altitude (see Fig. 5). Thus, it is absolutely necessary to correct for the stray light. The radiance comparisons against OSIRIS suggest that the algorithm presented in Sect. 2.3 is feasible.

In addition to the stray light, the signal saturates below around 30 km in the 400–500 nm region making a large part of the spectrum useless. Current saturation flags are not reliable, but the situation is greatly improved with the upcoming version of the Level 1 data.

The spectral resolution of GOMOS (bright limb signal) is poor, about 3.5 nm compared to the ∼1 nm resolution of OSIRIS. The spectra of GOMOS are also noisier than those of OSIRIS. Both the low spectral resolution and the noise make NO_2 retrievals difficult and so far it has not been successful.

Furthermore, there seems to be a systematic difference between the GOMOS and OSIRIS spectra in the wavelengths below 320 nm. This cannot be explained by the stray light because the discrepancy increases at lower altitudes where the relative amount of stray light decreases. The difference is apparent in both absolute and normalized radiance (see Figs. 6 and 8). Unfortunately, close matches between OSIRIS and GOMOS measurement times, tangent point locations, and solar angles are rare and only 14 cases were investigated in this paper.

The disagreement in the UV band leads to a difference in the retrieved ozone profiles between GOMOS bright limb and OSIRIS. It is possible to cope with the problem by suppressing the UV band in the retrieval below ∼40 km. After flagging the UV band (and the saturation band) the agreement with GOMOS night-time occultations was better than 10% between 22 and 50 km in the equator. The good comparison result against the GOMOS night-time occultations, after flagging the UV band, suggests that the UV band is biased indeed in GOMOS and not in OSIRIS.

Despite the weaknesses in the Level 1 data, the proposed stray light removal algorithm and the inversion method offer a promising way to utilize the whole GOMOS bright limb data set. The processing of the GBL data would roughly double the amount of useful GOMOS ozone profiles between at least 22 and 50 km. The distribution of GOMOS night-time and daytime measurements in 2004 is shown in Fig. 11.

Finally, it should be noted that the comparison for profiles shown in this paper is preliminary and should be extended using other reference instruments for all latitudes. Additionally, the robustness and performance of the stray light correction could be analyzed more carefully in a separate study.

Acknowledgements. This work was funded by the European Space Agency through the project *Trace Gas Retrieval from GOMOS Bright Limb Measurements* (AO/1-5301/06/I-OL) and by the Academy of Finland through the MIDAT project. The authors wish to thank Marko Laine, Seppo Hassinen, Benjamin Herman, Anne van Gijsel, and Ankie Piters for their valuable help. The authors also wish to thank the anonymous reviewers for their helpful comments and suggestions.

Edited by: C. von Savigny

References

Bourassa, A. E., Degenstein, D. A., and Llewellyn, E. J.: SASKTRAN: A spherical geometry radiative transfer code for efficient estimation of limb scattered sunlight, J. Quant. Spectrosc. Ra., 109, 52–73, doi:10.1016/j.jqsrt.2007.07.007, 2008.

Gillett, N. P., Akiyoshi, H., Bekki, S., Braesicke, P., Eyring, V., Garcia, R., Karpechko, A. Yu., McLinden, C. A., Morgenstern, O., Plummer, D. A., Pyle, J. A., Rozanov, E., Scinocca, J., and Shibata, K.: Attribution of observed changes in stratospheric ozone and temperature, Atmos. Chem. Phys., 11, 599–609, doi:10.5194/acp-11-599-2011, 2011.

Gottwald, M., Bovensmann, H., Lichtenberg, G., Noel, S., von Bargen, A., Slijkhuis, S., Piters, A., Hoogeveen, R., von Savigny, C., Buchwitz, M. A. K., Richter, A., Rozanov, A., Holzer-Popp, T., Bramstedt, K., Lambert, J.-C., Skupin, J., Wittrock, F., Schrijver, H., and Burrows, J.: SCIAMACHY, Monitoring the Changing Earth's Atmosphere, DLR, 2006.

Grant, W. B.: Ozone measuring Instruments for the Stratosphere, Optical Society of America, Washington, 1989.

Griffioen, E. and Oikarinen, L.: LIMBTRAN: A pseudo three-dimensional radiative transfer model for the limb-viewing imager OSIRIS on the Odin satellite, J. Geophys. Res., 105, 29717–29730, 2000.

Jones, A., Urban, J., Murtagh, D. P., Eriksson, P., Brohede, S., Haley, C., Degenstein, D., Bourassa, A., von Savigny, C., Sonkaew, T., Rozanov, A., Bovensmann, H., and Burrows, J.: Evolution of stratospheric ozone and water vapour time series studied

with satellite measurements, Atmos. Chem. Phys., 9, 6055–6075, doi:10.5194/acp-9-6055-2009, 2009.

Kiesewetter, G., Sinnhuber, B.-M., Weber, M., and Burrows, J. P.: Attribution of stratospheric ozone trends to chemistry and transport: a modelling study, Atmos. Chem. Phys., 10, 12073–12089, doi:10.5194/acp-10-12073-2010, 2010.

Kyrölä, E., Tamminen, J., Sofieva, V., Bertaux, J. L., Hauchecorne, A., Dalaudier, F., Fussen, D., Vanhellemont, F., Fanton d'Andon, O., Barrot, G., Guirlet, M., Fehr, T., and Saavedra de Miguel, L.: GOMOS O_3, NO_2, and NO_3 observations in 2002-2008, Atmos. Chem. Phys., 10, 7723–7738, doi:10.5194/acp-10-7723-2010, 2010.

Levenberg, K.: A Method for the Solution of Certain Problems in Least Squares, Quart. Appl. Math., 2, 164–168, 1944.

Llewellyn, E., Lloyd, N. D., Degenstein, D. A., Gattinger, R. L., Petelina, S. V., Bourassa, A. E., Wiensz, J. T., Ivanov, E. V., McDade, I. C., Solheim, B. H., McConnell, J. C., Haley, C. S., von Savigny, C., Sioris, C. E., McLinden, C. A., Griffioen, E., Kaminski, J., Evans, W. F. J., Puckrin, E., Strong, K., Wehrle, V., Hum, R. H., Kendall, D. J. W., Matsushita, J., Murtagh, D. P., Brohede, S., Stegman, J., Witt, G., Barnes, G., Payne, W. F., Piche, L., Smith, K., Warshaw, G., Deslauniers, D. L., Marchand, P., Richardson, E. H., King, R. A., Wevers, I., McCreath, W., Kyrölä, E., Oikarinen, L., Leppelmeier, G. W., Auvinen, H., Megie, G., Hauchecorne, A., Lefevre, F., de La Noe, J., Ricaud, P., Frisk, U., Sjoberg, F., von Scheele, F., and Nordh, L.: The OSIRIS instrument on the Odin spacecraft, Can. J. Phys., 82, 411–422, doi:10.1139/p04-005, 2004.

Marquardt, D.: An Algorithm for Least-Squares Estimation of Nonlinear Parameters, J. Soc. Indust. Appl. Math., 11, 431–44, 1963.

Meijer, Y. J., Swart, D. P. J., Allaart, M., Andersen, S. B., Bodeker, G., Boyd, I., Braathen, G., Calisesi, Y., Claude, H., Dorokhov, V., von der Gathen, P., Gil, M., Godin-Beekmann, S., Goutail, F., Hansen, G., Karpetchko, A., Keckhut, P., Kelder, H. M., Koelemeijer, R., Kois, B., Koopman, R. M., Kopp, G., Lambert, J.-C., Leblanc, T., McDermid, I. S., Pal, S., Schets, H., Stubi, R., Suortti, T., Visconti, G., and Yela, M.: Pole-to-pole validation of ENVISAT/GOMOS ozone profiles using data from ground-based and balloon-sonde measurements, J. Geophys. Res., 109, D23305, doi:10.1029/2004JD004834, 2004.

Oikarinen, L., Sihvola, E., and Kyrölä, E.: Multiple scattering radiance in limb-viewing geometry, J. Geophys. Res., 104, 31261–31274, 1999.

Pérot, K., Hauchecorne, A., Montmessin, F., Bertaux, J.-L., Blanot, L., Dalaudier, F., Fussen, D., and Kyrölä, E.: First climatology of polar mesospheric clouds from GOMOS/ENVISAT stellar occultation instrument, Atmos. Chem. Phys., 10, 2723–2735, doi:10.5194/acp-10-2723-2010, 2010.

Petelina, S., Llewellyn, E., Degenstein, D., and Lloyd, N.: Odin/OSIRIS limb observations of polar mesospheric clouds in 2001–2003, J. Atmos. Sol.-Terr. Phy., 68, 42–55, doi:10.1016/j.jastp.2005.08.004, 2006.

Postylyakov, O. V.: Radiative transfer model MCC++ with evaluation of weighting functions in spherical atmosphere for use in retrieval algorithms, Adv. Space Res., 34, 721–726, doi:10.1016/j.asr.2003.07.070, 2004.

Qu, J., Gao, W., Kafatos, M., Murphy, R., and Salomonson, V.: Earth Science Satellite Remote Sensing Vol. 1: Science and Instruments, Springer, Dordrecht, 2006.

Rault, D.: Ozone profile retrieval from Stratospheric Aerosol and Gas Experiment (SAGE III) limb scatter measurements, J. Geophys. Res., 110, D09309, doi:10.1029/2004JD004970, 2005.

Renard, J., Berthet, G., Brogniez, C., Catoire, V., Fussen, D., Goutail, F., Oelhaf, H., Pommereau, J., Roscoe, H. K., Wetzel, G., Chartier, M., Robert, C., Balois, J., Verwaerde, C., Auriol, F., François, P., Gaubicher, B., and Wursteisen, P.: Validation of GOMOS-Envisat vertical profiles of O_3, NO_2, NO_3, and aerosol extinction using balloon-borne instruments and analysis of the retrievals, J. Geophys. Res., 113, A02302, doi:10.1029/2007JA012345, 2008.

Robert, C. E., von Savigny, C., Burrows, J. P., and Baumgarten, G.: Climatology of noctilucent cloud radii and occurrence frequency using SCIAMACHY, J. Atmos. Sol.-Terr. Phy., 71, 408–423, doi:10.1016/j.jastp.2008.10.015, 2009.

Rozanov, E., Callis, L., Schlesinger, M., Yang, F., Andronova, N., and Zubov, V.: Atmospheric response to NO_y source due to energetic electron precipitation, Geophys. Res. Lett., 32, L14811, doi:10.1029/2005GL023041, 2005.

Shepherd, G. G.: Spectral Imaging of the Atmosphere, Academic Press, London, 2002.

Spada, F., Krol, M. C., and Stammes, P.: McSCIA: application of the Equivalence Theorem in a Monte Carlo radiative transfer model for spherical shell atmospheres, Atmos. Chem. Phys., 6, 4823–4842, doi:10.5194/acp-6-4823-2006, 2006.

Taha, G., Jaross, G., Fussen, D., Vanhellemont, F., Kyrölä, E., and McPeters, R. D.: Ozone profile retrieval from GOMOS limb scattering measurements, J. Geophys. Res., 113, D23307, doi:10.1029/2007JD009409, 2008.

Tamminen, J., Kyrölä, E., Sofieva, V. F., Laine, M., Bertaux, J.-L., Hauchecorne, A., Dalaudier, F., Fussen, D., Vanhellemont, F., Fanton-d'Andon, O., Barrot, G., Mangin, A., Guirlet, M., Blanot, L., Fehr, T., Saavedra de Miguel, L., and Fraisse, R.: GOMOS data characterisation and error estimation, Atmos. Chem. Phys., 10, 9505–9519, doi:10.5194/acp-10-9505-2010, 2010.

Tukiainen, S., Hassinen, S., Seppälä, A., Auvinen, H., Kyrölä, E., Tamminen, J., Haley, C. S., Lloyd, N., and Verronen, P. T.: Description and validation of a limb scatter retrieval method for Odin/OSIRIS, J. Geophys. Res., 113, D04308, doi:10.1029/2007JD008591, 2008.

van Gijsel, J. A. E., Swart, D. P. J., Baray, J.-L., Bencherif, H., Claude, H., Fehr, T., Godin-Beekmann, S., Hansen, G. H., Keckhut, P., Leblanc, T., McDermid, I. S., Meijer, Y. J., Nakane, H., Quel, E. J., Stebel, K., Steinbrecht, W., Strawbridge, K. B., Tatarov, B. I., and Wolfram, E. A.: GOMOS ozone profile validation using ground-based and balloon sonde measurements, Atmos. Chem. Phys., 10, 10473–10488, doi:10.5194/acp-10-10473-2010, 2010.